LABORATORY INVESTIGATION

In Vivo Fluorescence Microendoscopic Monitoring of Stent-Induced Fibroblast Cell Proliferation in an Esophageal Mouse Model

Eun Jung Jun, PhD, Ho-Young Song, MD, Jung-Hoon Park, PhD, Yoon Sung Bae, PhD, Bjorn Paulson, PhD, Sanghwa Lee, PhD, Young Chul Cho, MS, Jiaywei Tsauo, MD, Min Tae Kim, MS, Kun Yung Kim, MD, Su-Geun Yang, PhD, and Jun Ki Kim, PhD

ABSTRACT

Purpose: To evaluate the feasibility of self-expanding metal stent (SEMS) placement and fluorescence microendoscopic monitoring for determination of fibroblast cell proliferation after stent placement in an esophageal mouse model.

Materials and Methods: Twenty fibroblast-specific protein (FSP)-1 green fluorescent protein (GFP) transgenic mice were analyzed. Ten mice (Group A) underwent SEMS placement, and fluoroscopic and fluorescence microendoscopic images were obtained biweekly until 8 weeks thereafter. Ten healthy mice (Group B) were used for control esophageal values.

Results: SEMS placement was technically successful in all mice. The relative average number of fibroblast GFP cells and the intensities of GFP signals in Group A were significantly higher than in Group B after stent placement. The proliferative cellular response, including granulation tissue, epithelial layer, submucosal fibrosis, and connective tissue, was increased in Group A. FSP-1-positive cells were more prominent in Group A than in Group B.

Conclusions: SEMS placement was feasible and safe in an esophageal mouse model, and proliferative cellular response caused by fibroblast cell proliferation after stent placement was longitudinally monitored using a noninvasive fluorescence microendoscopic technique. The results have implications for the understanding of proliferative cellular response after stent placement in real-life patients and provide initial insights into new clinical therapeutic strategies for restenosis.

ABBREVIATIONS

α-SMA = alpha-smooth muscle actin, ECM = extracellular matrix, FSP = fibroblast-specific protein, GFP = green fluorescent protein, GRIN = gradient-index, PMT = photomultiplier tub, SEMS = self-expanding metal stent

For the last 2 decades, self-expanding metal stents (SEMSs), including bared or covered stents, have been used as an effective alternative therapeutic option in the treatment of esophageal strictures (1–4). However, the development of new stricture as a result of a proliferative cellular response to the mechanical pressure of the stent on the luminal wall has been a major disadvantage in stent placement in the esophagus, as well as in the urethra and trachea (3–6). Recently, biodegradable stents have become available for the clinical treatment of benign gastrointestinal strictures (7–10). Despite the effectiveness of biodegradable stents in dilating strictures, and even despite their theoretical biocompatibility, they may not be able to forestall the development of hyperplastic strictures, and their real effectiveness and safety are not yet certain. Stent placement into the esophagi of rats, rabbits, and pigs has been shown to

From the Departments of Radiology (E.J.J., H.-Y.S., J.-H.P., Y.C.C., J.T., M.T.K., K.Y.K.), Biomedical Engineering Research Center (J.-H.P., Y.S.B., B.P., S.L., J.K.K.), and Convergence Medicine, Asan Medical Center, University of Ulsan College of Medicine, 88, Olymic-ro 43-gil, Songpa-gu, Seoul, Republic of Korea; Department of Physics (B.P.), College of Science, Yonsei University, Seoul, Republic of Korea; and Department of New Drug Development and NCEED (S.-G.Y.), School of Medicine, Inha University, Incheon, Republic of Korea. Received February 27, 2018; final revision received June 25, 2018; accepted June 29, 2018. **Address correspondence to** J.K.K.; E-mail: kim@amc.seoul.kr

E.J.J. and H.-Y.S. contributed equally to this work and are co-first authors.

None of the authors have identified a conflict of interest.

J Vasc Interv Radiol 2018; ■:1–8

https://doi.org/10.1016/j.jvir.2018.06.024

reproduce the mechanisms of restenosis in humans (11–16). However, these animal models are only available in limited transgenic variants and have high associated costs that limit their applicability for teasing out the molecular pathways of restenosis. Furthermore, they are only available in a limited number of laboratories and may require high drug dosages in future experimental studies of drug-delivering SEMSs.

Proliferative cellular response is the hallmark of tissue repairs and consists of proliferating fibroblasts and migrating epithelial cells (14,17). Fibroblasts play a central role in proliferative cellular responses at a cellular level (18–21). In vivo fluorescence microendoscopy techniques have been proposed to monitor pathologic changes in live mice over long periods (22–24), in a minimally invasive manner. To investigate the role of fibroblast proliferation in stent-induced restenosis by fluorescence microendoscopy, transgenic mice were bred featuring green fluorescent protein (GFP)-expressing fibroblast cells. SEMSs suitable for an esophageal mouse model and a placement technique were developed.

In this study, the feasibility of SEMS placement and fluorescence microendoscopic monitoring of fibroblast proliferation after stent placement in an esophageal mouse model was developed for insights into the mechanisms behind complications experienced in stent treatment of real-life clinical patients. The first demonstration of a mouse esophageal stent model using a noninvasive fluorescence microendoscopic technique for monitoring of stent-induced fibroblast cell proliferation is presented. By using fluorescence microendoscopy, the relative average number and fluorescence intensities of fibroblast GFP cells were compared between the stented and control esophagus models using fibroblast-specific protein-1 (FSP-1) GFP transgenic mice (25). The purpose of this study was to evaluate the feasibility of SEMS placement and fluorescence microendoscopic monitoring of fibroblast proliferation after stent placement in an esophageal mouse model that could replicate human changes and provide insights into clinical therapeutic strategies for real-life patients.

MATERIALS AND METHODS

This study was approved by the Institutional Animal Care and Use Committee and conformed to US National Institutes of Health guidelines for the humane handling of laboratory animals.

Animal Study

A total of 20 FSP-1 transgenic mice weighing 20–25 g (25) were included for study. Ten of the 20 FSP-1 GFP transgenic mice (Group A) randomly underwent SEMS placement, and fluoroscopic and fluorescence microendoscopic images were obtained 2, 4, 6, and 8 weeks thereafter. The remaining 10 healthy FSP-1 GFP transgenic mice (Group B), which also underwent fluoroscopic and fluorescence microendoscopic evaluation, were used for control values of the esophagus. All mice were euthanized 8 weeks after stent placement by administering inhalable pure carbon dioxide.

Stent Construction and Placement

The SEMS (Taewoong, Gyunggi, Korea) was knitted from a single thread of 0.1-mm-thick nitinol wire filament in a tubular configuration with 6 bent points on the upper and lower ends. When fully expanded, the stent was 3 mm in diameter and 5 mm in length. Two radiopaque makers at each end of the stent facilitated precise placement.

Anesthesia was induced through intramuscular injection of 50 mg/kg zolazepam and tiletamine (Zoletil 50; Virbac, Carros, France) and 10 mg/kg xylazine (Rompun; Bayer HealthCare, Leverkusen, Germany). A 0.014-inch microguidewire (Transcend; Boston Scientific, Watertown, Massachusetts) was inserted under fluoroscopic guidance, and a 4-Fr sheath and a dilator were advanced over the guidewire into the lower esophagus. With the sheath left in place, the guidewire and dilator were removed in all mice. In Group A, a compressed stent was loaded into the 1.2-mm-diameter sheath and positioned in the esophagus with the use of a pusher catheter under fluoroscopic guidance. The stent was deployed at the mid-thoracic esophagus by withdrawing the sheath as the pusher catheter was held in place. The sheath and the pusher catheter were pulled out of the esophagus after stent placement (**Fig 1**). In Group B, the stent placement procedure was omitted.

Optical Probe and Imaging System

A miniaturized microendoscope using a gradient-index (GRIN) lens (NSG America, Somerset, New Jersey) was constructed and combined with a home-built confocal microendoscope system (**Fig 2**) (22). The microendoscope has an outer diameter of 1.2 mm, including a stainless metal sheath sleeved over the probe that protects the GRIN lens glass mechanically. For side-view imaging, a microprism mirror was attached to the distal end of the focusing lens. The imaging probe was integrated into a laser-scanning confocal microscope with a rotational mount (Thorlabs, Newton, New Jersey) (22).

Fluorescence Microendoscopic Monitoring of Fibroblast GFP Cells

To obtain fluorescence images, the mice were anaesthetized and placed on a body temperature-maintaining platform on a 3-dimensional translation stage (Sutter MP285 motorized micromanipulator; Sutter, Novato, California). The tongue was gently pulled out from the mouse for smooth insertion of the endoscope and to secure the airway simultaneously. The fluorescence microendoscope was inserted through the mouth into the proximal end of the stent. For real-time intravital imaging, the scanning speed of a home-built laser scanning confocal system was adjusted to a frame rate of 30 Hz. The scan range was 15 mm, including around

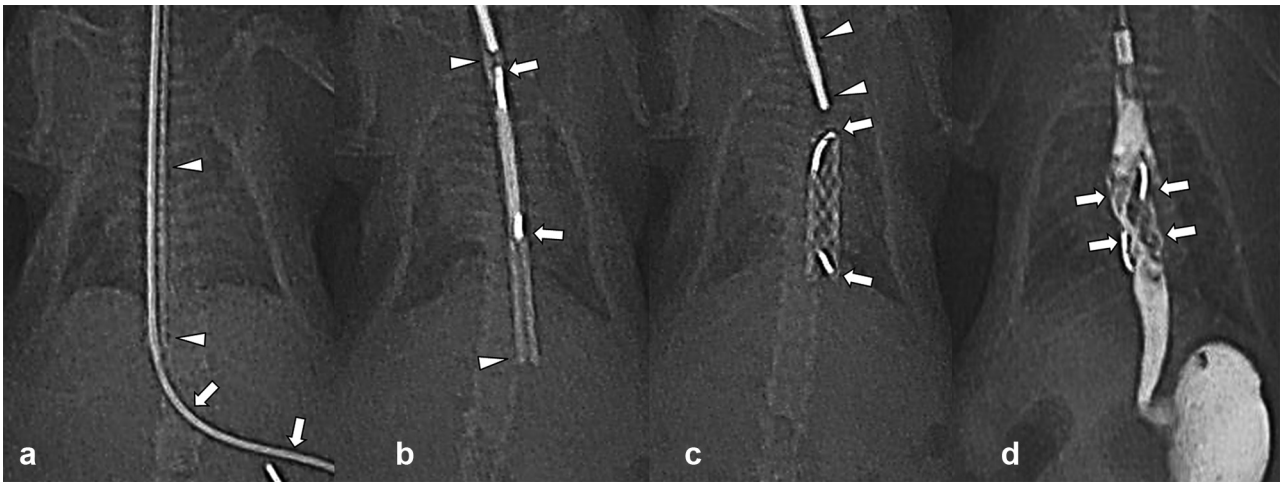

Figure 1. Radiographic images showing the technical steps of **s**tent placement and representative follow-up esophagography. (**a**) A micro-guidewire (arrows) is inserted through the esophagus into the stomach, and a 4-Fr sheath and a dilator (arrowheads) are advanced over the guidewire. (**b**) A compressed stent (arrows) inside the 4-Fr sheath (arrowheads). (**c**) The stent (arrows) is placed with the use of a pusher catheter (arrowheads) under fluoroscopic guidance. (**d**) Follow-up esophagograph obtained 8 weeks after stent placement showing a filling defect (arrows) caused by proliferative cellular responses.

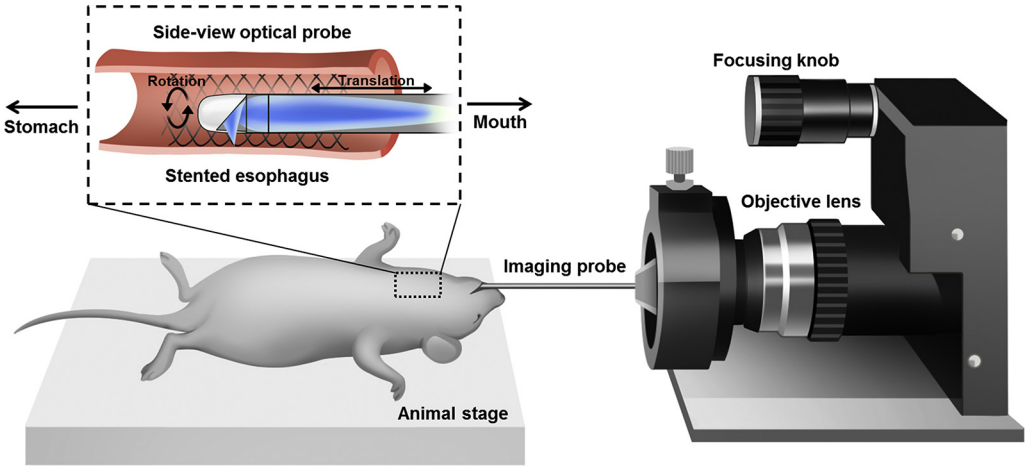

Figure 2. Schematic images are demonstrating in vivo endo-esophageal fluorescence microscopic imaging system.

5 mm past the proximal and distal ends of the 5-mm stent. The 488-nm laser sources for visualizing fibroblast cells of mice were maintained at the same power, and photomultiplier tube (PMT) conditions were maintained at the same sensitivity. At the completion of every imaging procedure, the optical probe was gently removed from the esophagus, and the mouse was allowed to recover on a heating stage. Fluorescence microendoscopic monitoring of fibroblast GFP cells was performed before stent placement and biweekly until 8 weeks thereafter at the same esophageal segments in all groups. To maintain similar GFP cell intensity conditions for comparison, laser power and PMT sensitivity were kept constant during each imaging session.

During imaging, frame averaging (typically 90–120 frames) was applied to reduce the noise level of acquired frames. In post-processing, the relative cell numbers and intensities of fibroblast GFP cells were measured using an automated cell-counting algorithm written in MATLAB. Background intensity variations were minimized with Gaussian filtering to remove shot noise, and disk-shaped morphologic structuring elements reduced the larger-scale intensity variations due to out-of-focus tissues (26). Boundary detection based on Otsu's thresholding algorithm was used to determine cell numbers (27), and the resulting cell boundaries were used to calculate the average intensities of fibroblast GFP cells, which are a marker for cell health.

Esophagographic Examination

Esophagography was performed just before sacrifice in all mice to verify the position and patency of the stent using a fluoroscopic machine (Artis Zee Multipurpose; Siemens, Munich, Germany). All esophagographies were conducted with use of contrast media (Ompipaque 300; GE Healthcare, Cork, Ireland) and a calibrated catheter to measure the inner luminal diameter of the stented esophagus. The inner

luminal diameter was digitally measured on each esohpagograph (Photoshop, version 6.0; Adobe Systems, Palo Alto, California). The stented esophagus was portioned into 3 segments: proximal, middle, and distal. Esophageal stenosis resulting from the proliferative cellular response in the SEMS was graded as follows: grade 0, defined as normal; grade 1, mild esophageal wall irregularity; grade 2, filling defect of $< 50\%$ of the stent diameter; and grade 3, filling defect of $> 50\%$ of the stent diameter. The esophagographic findings were analyzed on the consensus of 3 observers.

Histologic Examination

Surgical exploration of the esophagus and stomach was followed by gross examination to evaluate the degree of proliferative cellular response and to determine possible esophageal injury after stent placement. Stented esophagi were sectioned transversely at the proximal and distal regions. Tissue samples were fixed in 10% neutral buffered formalin for 24 hours and embedded in paraffin and sectioned. Samples were stained with hematoxylin and eosin and Masson's trichrome. Histologic evaluation with hematoxylin and eosin included determining the degree of submucosal inflammatory cell infiltration, the number of epithelial layers, the thickness of submucosal fibrosis, and the granulation tissue-related percentage of the esophageal cross-sectional area of stenosis calculated as 100 × (1-(stenotic stented area/original stented area)). The degree of inflammatory cell infiltration was subjectively determined according to the distribution and density of the inflammatory cells (graded as 1, mild; 2, mild to moderate; 3, moderate; 4, moderate to severe; and 5, severe). The average values of the histologic evaluation represented the average of 8 points around the circumference. The percentage of connective tissue area was determined using Masson's trichrome-stained sections. The connective tissue (collagen) area was calculated as follows: 100 × (1-(connective area/original area)). Histologic analysis of the esophagus was performed with a BX51 microscope (Olympus, Tokyo, Japan). Image-Pro Plus (Media Cybernetics, Silver Spring, Maryland) was used for measurements.

Immunohistochemical analysis was performed with alpha-smooth muscle actin (α-SMA) and collagen-1 as the primary antibodies (Abcam, Cambridge, United Kingdom). The sections were visualized with a NexES IHC automatic immunohistochemical stainer (Ventana Medical Systems, Tucson, Arizona).

Histologic findings were assessed by the consensus of 3 observers blinded to group assignments.

Immunofluorescence Analysis

The stented esophagus was harvested and fixed by immersion in 4% paraformaldehyde containing perfusion buffer at 4°C, followed by sequential incubation in 15% and 30% sucrose solution. Then, the fixed samples were embedded in Optimal cutting temperature compound (Agar Scientific), and 6-μm cryostat sections were prepared and collected on slides for the subsequent staining steps. Immunofluorescence staining was performed with FSP-1 (Abcam) antibody and Alexa Flour 488 (ThermoFisher Scientific, Waltham, Massachusetts).

Statistical Analysis

Data are expressed as mean ± standard deviation. Comparisons between stented and control esophagi were performed using Student's *t*-test. *P* values less than .05 were considered statistically significant. Statistical analyses were performed with SPSS software, version 22.0 (SPSS, IBM Corp, Chicago, Illinois).

RESULTS

Stent placement was technically successful in all mice. One of 10 (10%) mice died during fluorescence microendoscopic monitoring because of breathing difficulty, and stent migration distally into the stomach occurred 2 weeks after stent placement in 1 mouse. These 2 mice were excluded from the study. The remaining 8 mice survived until the end of the study with no stent-related complications.

Monitoring of Fibroblast GFP Cells

The time-lapse fluorescence images of the fibroblast-GFP cells are presented in **Figure 3**. The fluorescence images in Group A showed that the number of fibroblast cells increased after stent placement and peaked at 2 weeks (**Fig 3a**). The relative average number of the fibroblast GFP cells was significantly higher in Group A than in Group B at 2, 4, 6, and 8 weeks after stent placement ($P = .041$, .033, .010, and .014, respectively) (**Fig 3b**). The relative average intensities of the GFP signals in Group A were also significantly higher than in Group B for all measurements after stent placement ($P = .043$, .016, .042, and .008, respectively) (**Fig 3c**).

Esophagographic Findings

The overall average luminal diameter of Group A was 1.75 ± 0.15 mm (2.03 ± 0.17 mm in the proximally stented segment, 1.68 ± 0.13 mm in the middle stented segment, and 1.54 ± 0.15 mm in the distally stented segment). The median grade of proliferative cellular response after stenting was 3 (grade 1 in 1 mouse, grade 2 in 2 mice, and grade 3 in the remaining 5 mice).

Histologic Findings

The histologic findings after sacrifice are shown in **Figure 4** and **Table**. The mean granulation tissue (61.91% ± 15.28%) of the original esophageal lumen and the mean inflammatory cell infiltration were observed (moderate to severe; 3.9 ± 1.02) in Group A. Furthermore, the mean number of epithelial layers (3.8 ± 0.9) and the mean thickness of submucosal fibrosis (0.87 ± 0.26 mm) were increased

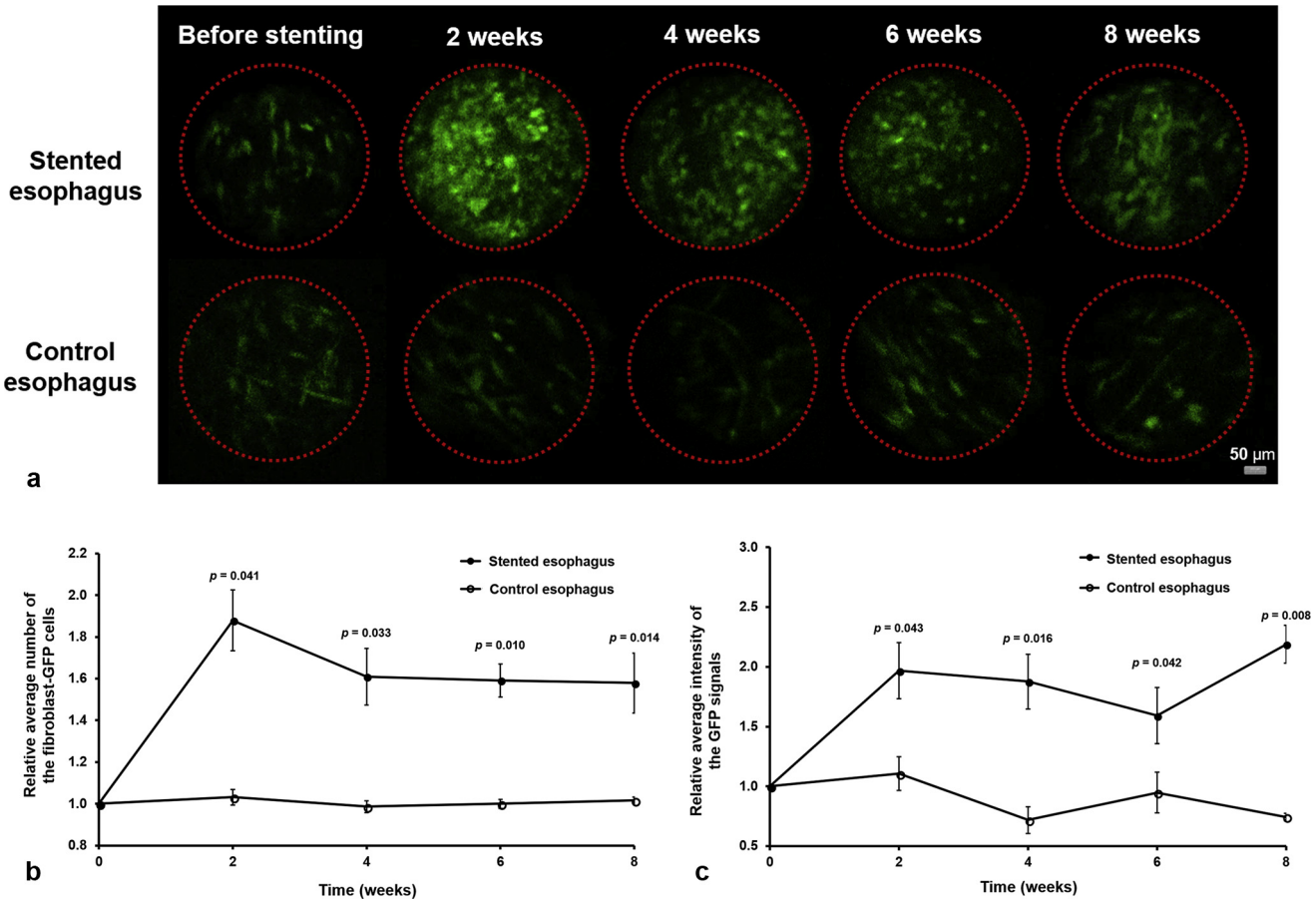

Figure 3. The relative average number of fibroblast GFP cells and the intensities of the GFP signals in the stented esophagus were significantly higher than those in the control esophagus. (**a**) Time-lapse fluorescence images of fibroblast GFP cells in vivo before and 2, 4, 6, and 8 weeks after stent placement. (**b**) Relative average number of the counted fibroblast GFP cells. Error bars = 95% confidence interval (CI). (**c**) Changes of the relative average intensity in the GFP cells. Error bars = 95% CI.

after stent placement compared to Group B (1.3 ± 0.5 and 0.04 ± 0.00 mm). The mean percentage of connective tissue area was 43.56 ± 6.83%, indicating submucosal collagen deposition.

The FSP-1 positive cells were more prominent in Group A than in Group B. The protein levels of collagen-1 and α-SMA also increased after stent placement.

DISCUSSION

There is a serious need for an easily manipulable animal model to screen stents and gain insight into the pathobiological mechanisms of tissue hyperplasia in nonvascular luminal structures. The results of this study demonstrated that stent placement into the esophagi of mice was technically successful, although procedural complications occurred due to stent migration and in vivo endoscopy. Combined with in vivo molecular imaging, biological analysis can be performed during stent placement, removal, and degradation. The model allows investigation into the molecular pathways of in-stent restenosis, beyond that possible in human patients, due to the availability of appropriate antibodies, transgenic strains, and knockout strains in mice. Consequently, the mouse model would allow anatomic and biological studies related to esophageal stent complications, using only restrictive methods, (11,12) and allows side-by-side evaluation of new therapeutic strategies for preventing long-term stent migration and reversing stent-induced tissue hyperplasia in real-life patients (28).

The imaging system using FSP-1 GFP transgenic mice was provided to visualize the increase of fibroblast GFP cells after stent placement in a live mouse. In vivo imaging systems have several advantages over cellular counting ex vivo after animal sacrifice. First, longitudinal monitoring may reduce the statistical errors from each animal's variability. Second, a smaller number of animals is generally required to achieve equivalent accuracy with histologic analysis (23,24). Third, and most importantly, the ability to comprehensively image the entire epithelium over a long segment of esophagus provides information about the spatial distribution, population, proliferation, and migration of cells, which are often difficult to obtain from tissue sections.

Proliferative cellular response occurs as an excessive response to mechanical injury after stent placement and has previously been the greatest hurdle in the management of

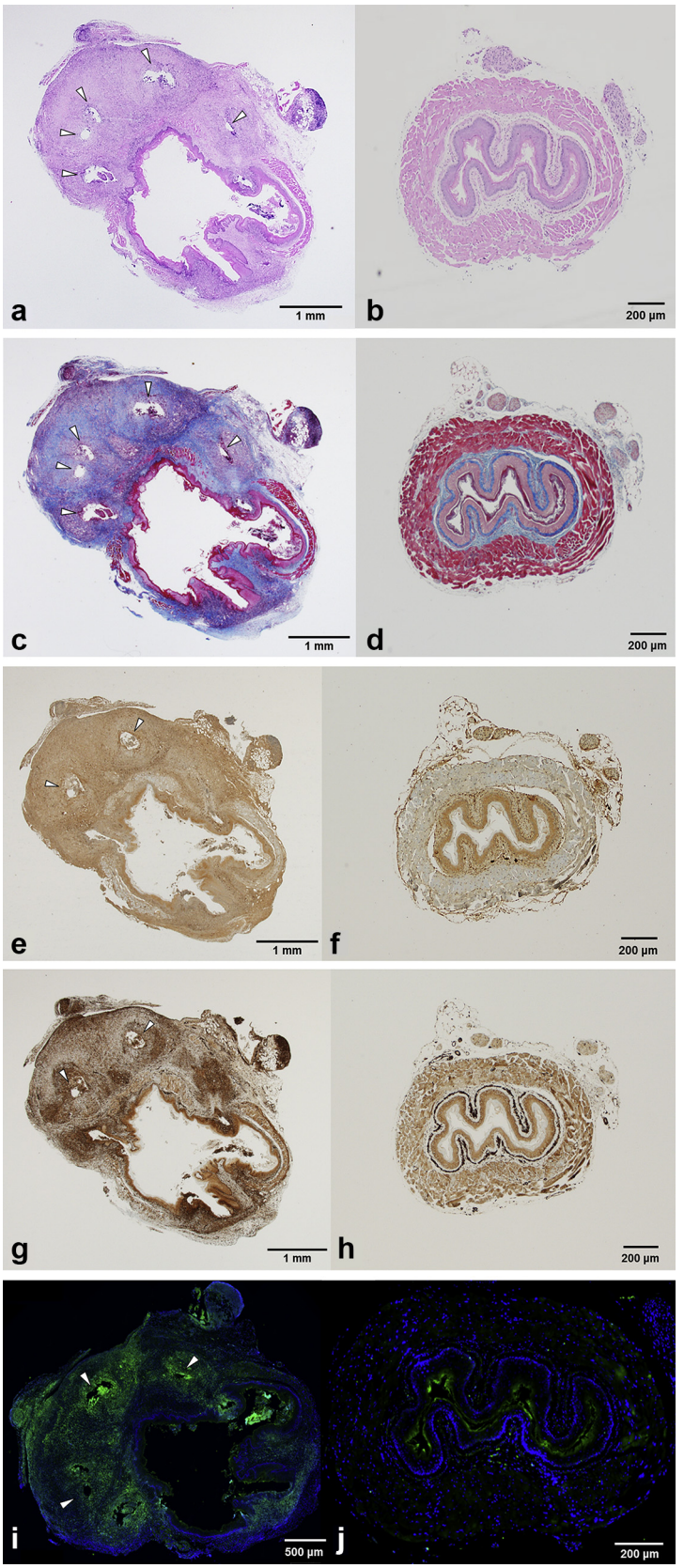

Figure 4. Representative microscopic images of histologic sections for stented esophagus (Group A: a, c, e, g; scale bars = 1 mm and i; scale bars = 500 μm) and control esophagus (Group B: b, d, f, g, j; scale bars = 200 μm). Hematoxylin and eosin (**a, b**), Masson's trichrome (**c, d**). Immunohistochemical analysis of collagen-1 (**e, f**), α-SMA (**g, h**), and FSP-1 immunofluorescence (4′,6-diamidino-2-phenylindole; blue, FSP-1; green) (**i, j**). Arrowhead = stent struts.

Table. Histopathologic Findings

	Percentage of granulation tissue area (%)	Inflammatory cell infiltration (grade)	Number of epithelial layers (number)	Thickness of submucosal fibrosis (mm)
Group A	61.91 ± 15.28	3.9 ± 1.02	3.8 ± 0.9	0.87 ± 0.26
Group B			1.3 ± 0.5	0.04 ± 0.00

benign strictures in nonvascular luminal organs (3,5,6). The major mechanism of stent-induced proliferative cellular response is re-epithelialization and fibroplasia (14). Epithelial-mesenchymal transition inducers are associated with dramatic changes in extracellular matrix (ECM) composition, and the ECM of proliferative cellular response is created and modified by fibroblasts (29–31). Furthermore, fibroblasts have a high capacity to synthesize ECM components and stimulate production of collagen (19–21). In this study, the relative average number of the fibroblast GFP cells and the intensities of the GFP signals in the stented esophagus increased significantly over those in the control, and they did so immediately after stent placement, peaking within 2 weeks. Concurrently, immunofluorescence analysis showed that FSP-1 was more prominent in the stented esophagus than in the control esophagus.

The observed fluorescence signal was consistent with a standard division of the wound-healing process after mechanical injury into inflammatory, fibroblastic, and granulation phases within approximately 4 weeks. Early on, fibroblasts and epithelial cells migrate to the wound site, where they form highly vascular proliferative cellular responses. Fibroblasts in proliferative cellular responses transform into myofibroblasts, and eventually the lesion evolves into a scar with dense collagen and greatly reduced vascularity and cellularity.

The luminal diameter of the stented esophagus decreased over 8 weeks after stent placement, indicating a stent-induced proliferative cellular response. Nodularity and smoothness were regarded as representative components denoting tissue hyperplasia secondary to stent placement (1,2,15). Nodularity was defined as a nodular contour of the esophageal mucosa and was considered to represent tissue hyperplasia, whereas smoothness was defined as the absence of such nodular contours (15,32). Gross examinations were performed to evaluate tissue hyperplasia and esophageal injuries, such as perforation or inflammation. Histopathologic findings also revealed that the granulation tissue area, the number of epithelial layers, the submucosal fibrosis thickness, and the connective tissue area were increased, which correlated with esophagography findings. Furthermore, the FSP-1-positive cells (a marker of fibroblasts) were more prominent in the stented esophagus, and the protein levels of collagen-1 (a marker of connective tissues) and α-SMA (a mesenchymal cell marker) were also increased after stent placement. These results provide convincing evidence that the esophageal mouse model is easy to evaluate, may be relevant to biological and histologic studies, and thus will be useful for investigations on many types of stent placement.

This study had some limitations. First, although fluorescence microendoscopic long-term monitoring was successfully performed, the number of study mice was small. Second, histopathologic analysis was not performed at 2, 4, and 6 weeks after stent placement. Furthermore, wound healing after mechanical injury secondary to stent placement may differ considerably between control and stricture tissue. Third, although representative markers of ECM and fibrosis were evaluated in this study, more precise biological markers should be targeted for further insight into the origins and treatment of the proliferative cellular response. Finally, this experiment ended after a period of only 8 weeks and without monitoring after stent removal. The reversibility of the observed cellular proliferation remains to be observed in subsequent mural experiments.

This study demonstrated the first SEMS placement in an esophageal mouse model as a new minimally invasive approach with low stent-related complications and procedure-related death. In vivo long-term molecular monitoring of proliferative cellular response using a fluorescence microendoscopic technique was successfully performed. In conclusion, placement of SEMS was feasible and safe in an esophageal mouse model, and proliferative cellular response caused by fibroblast proliferation after stent placement was longitudinally monitored using a noninvasive fluorescence microendoscopic technique. The tools presented in this article may allow an investigation into molecular pathways in gastrointestinal tract disease progression in vivo and could be promising as a starting point for addressing clinical problems.

ACKNOWLEDGMENTS

This study was supported by the Basic Science Research Program (2014R1A1A2057773, 2015K2A7A1035896) and MRC grant (2018R1A5A2020732) through the National Research Foundation of Korea, funded by the Ministry of Science & ICT and the Ministry of Trade, Industry & Energy, under Industrial Technology Innovation Program (10080726, 10052048, 20000843). This study was also supported by a grant (2015-055, 2015-641, 2015-646) from the Asan Institute for Life Sciences, Asan Medical Center, Seoul, Korea.

REFERENCES

1. Boyce HW Jr. Stents for palliation of dysphagia due to esophageal cancer. N Engl J Med 1993; 329:1345–1346.
2. Song HY, Do YS, Han YM, et al. Covered, expandable esophageal metallic stent tubes: experiences in 119 patients. Radiology 1994; 193:689–695.
3. Kim JH, Song HY, Choi EK, et al. Temporary metallic stent placement in the treatment of refractory benign esophageal strictures: results and factors associated with outcome in 55 patients. Eur Radiol 2009; 19: 384–390.
4. Park JH, Song HY, Kim JH, et al. Polytetrafluoroethylenope-covered retrievable expandable nitinol stents for malignant esophageal obstructions: factors influencing the outcome of 270 patients. AJR Am J Roentgenol 2012; 199:1380–1386.

5. Song HY, Park H, Suh TS, et al. Recurrent traumatic urethral strictures near the external sphincter: treatment with a covered, retrievable, expandable nitinol stent–initial results. Radiology 2003; 226:433–440.
6. Kim JH, Shin JH, Song HY, et al. Benign tracheobronchial strictures: long-term results and factors affecting airway patency after temporary stent placement. AJR Am J Roentgenol 2007; 188:1033–1038.
7. Dumoulin FL, Plassmann D. Tissue hyperplasia following placement of a biodegradable stent for a refractory esophageal stricture: treatment with argon plasma coagulation. Endoscopy 2012; 44:E356–E357.
8. Fischer A, Bausch D, Baier P, Braun A, Richter-Schrag H. Risk of biodegradable stent-induced hypergranulation causing re-stenosis of a gastric conduit after esophageal resection. Endoscopy 2012; 44:E125–E126.
9. Hair CS, Devonshire DA. Severe hyperplastic tissue stenosis of a novel biodegradable esophageal stent and subsequent successful management with high-pressure balloon dilation. Endoscopy 2010; 42: E132–E133.
10. Orive-Calzada A, Alvarez-Rubio M, Romero-Izquierdo S, et al. Severe epithelial hyperplasia as a complication of a novel biodegradable stent. Endoscopy 2009; 4:E137–E138.
11. Zhu YQ, Edmonds L, Wei LM, et al. Technical feasibility and tissue reaction after silicone-covered biodegradable magnesium stent insertion in the oesophagus: a primary study in vitro and in vivo. Eur Radiol 2017; 27: 2546–2553.
12. Feng Y, Jiao C, Cao Y, et al. A comparison of a fully covered and an uncovered segmented biodegradable esophageal stent in a porcine model: preclinical evaluation of degradation, complications, and tissue reactions. Gastroenterol Res Pract 2016; 2016:8690858.
13. Kim EY, Song HY, Kim JH, et al. IN-1233-eluting covered metallic stent to prevent hyperplasia: experimental study in a rabbit esophageal model. Radiology 2013; 267:396–404.
14. Jun EJ, Park JH, Tsauo J, et al. EW-7197, an activin-like kinase 5 inhibitor, suppresses granulation tissue after stent placement in rat esophagus. Gastrointest Endosc 2017; 86:219–228.
15. Kim EY, Shin JH, Jung YY, et al. A rat esophageal model to investigate stent-induced tissue hyperplasia. J Vasc Interv Radiol 2010; 21: 1287–1291.
16. Wang Z, Liu J, Wu K, et al. Nitinol stents loaded with a high dose of antitumor 5-fluorouracil or paclitaxel: esophageal tissue responses in a porcine model. Gastrointest Endosc 2015; 82:153–160.
17. Werner S, Krieg T, Smola H. Keratinocyte-fibroblast interactions in wound healing. J Invest Dermatol 2007; 127:998–1008.
18. Park JH, Kim JH, Kim EY, et al. Bioreducible polymer-delivered siRNA targeting MMP-9: suppression of granulation tissue formation after bare metallic stent placement in a rat urethral model. Radiology 2014; 271: 87–95.
19. Leask A, Abraham DJ. TGF-β signaling and the fibrotic response. FASEB J 2004; 18:816–827.
20. Frangogiannis NG. Targeting the inflammatory response in healing myocardial infarcts. Curr Med Chem 2006; 13:1877–1930.
21. Lindley LE, Briegel KJ. Molecular characterization of TGFb-induced epithelial-mesenchymal transition in normal finite lifespan human mammary epithelial cells. Biochem Biophys Res Commun 2010; 399: 659–664.
22. Kim JK, Lee WM, Kim PH, et al. Fabrication and operation of GRIN probes for in vivo fluorescence cellular imaging of internal organs in small animals. Nat Protoc 2012; 7:1456–1469.
23. Kim JK, Vinarsky V, Wain J, et al. In vivo imaging of tracheal epithelial cells in mice during airway regeneration. Am J Respir Cell Mol Biol 2012; 47: 864–868.
24. Choi JW, Kim JK, Choi MH, et al. In vivo imaging of Lgr5-positive cell populations using confocal laser endomicroscopy during early colon tumorigenesis. Endoscopy 2014; 46:1110–1116.
25. Iwano M, Plieth D, Danoff TM, et al. Evidence that fibroblasts derive from epithelium during tissue fibrosis. J Clin Invest 2002; 110:341–350.
26. Tyack PL, Calambokidis J, Friedlaender A, et al. Formal Comment on Schorr GS, Falcone EA, Moretti DJ, Andrews RD (2014). First long-term behavioral records from Cuvier's beaked whales (Ziphius cavirostris) reveal record-breaking dives. PLoS One 2015; 9: e92633.
27. Al-Khazraji BK, Medeiros PJ, Novielli NM, et al. An automated cell-counting algorithm for fluorescently-stained cells in migration assays. Biol Proced Online 2011; 13:9.
28. Vandamme T. Use of rodents as models of human diseases. J Pharm Bioallied Sci 2014; 6:2.
29. Taylor MA, Parvani JG, Schiemann WP, et al. The pathophysiology of epithelial–mesenchymal transition induced by transforming growth factor-β in normal and malignant mammary epithelial cells. J Mammary Gland Biol Neoplasia 2010; 15:169–190.
30. Okada H, Danoff TM, Kalluri R, et al. Early role of Fsp1 in epithelial-mesenchymal transformation. Am J Physiol 1997; 273:563–574.
31. Polyak K, Weinberg RA. Transitions between epithelial and mesenchymal states: acquisition of malignant and stem cell traits. Nat Rev Cancer 2009; 9:265–273.
32. Shin JH, Lee SK, Song HY, et al. The effects of 188 rhenium-filled balloon dilation following bare stent placement in a rabbit oesophageal model. Br J Radiol 2008; 81:413–421.